Applied Physics B
Lasers and Optics

CrossMark

Optical properties of point-defect nanocavity implemented in planar photonic crystal with various low refractive index cladding materials

Lazhar Kassa-Baghdouche[1,2] · Touraya Boumaza[2] · Mohamed Bouchemat[2]

© Springer-Verlag Berlin Heidelberg 2015

Abstract This paper presents a theoretical investigation of the optical properties of a three missing holes point-defect cavity implemented in a planar photonic crystal with various low refractive index cladding materials. To describe the cavity operation, we analyze how the refractive index (RI) of the cladding material depends on the Q factor and resonant wavelength for both asymmetric and symmetric structures. The results show that the radiation losses of the structures increase for decreasing RI contrast and that the Q factor drops dramatically. We show that the periodicity of the RI of the cladding material is a critical consideration for realizing symmetric structures with high-Q factors. Furthermore, we fine-tune the radius and position of the lateral-, upper-, and lower-boundary holes near the cavity edges, which allows us to increase the Q factor of the planar photonic crystal cavity by a factor as large as 25 ($Q > 10^4$). These findings provide useful design rules for applications involving mechanically stable photonic crystal cavities with high-Q factors.

1 Introduction

Photonic crystals (PhCs) have attracted significant interest because of their many applications in integrated optics. One well-known class of PhC structure is two-dimensional (2D) planar PhCs, which have 2D periodicity in the membrane plane [1]. Such structures feature in-plane optical confinement, which is based on the 2D photonic bandgap (PBG) effect and on vertical confinement resulting from the high contrast between the refractive index (RI) of the dielectric membrane and that of the surrounding (bottom and top) claddings. Although air-bridge structures are effective for making advanced integrated optical components, such as single-photon emitters [2, 3], low-threshold nanolasers [4–6], ultrasmall filters [7], ultralow-power and ultrafast switches [8], and highly efficient single-quantum-dot emitters [9–12], their poor mechanical stability, high thermal resistance, complex fabrication requirements, and vulnerability to contamination are major obstacles to heat management and heterogeneous integration. Furthermore, when 2D PhCs are fully cladded by air, continuous oxidation and unavoidable contamination can affect the structural characteristics of the photonic device [13]. To address these problems, various investigations have focused on planar PhC nanocavities partially or fully clad by low-RI materials [14–23].

In particular, cavities made of planar PhCs with three missing holes linearly arranged (L3) are attracting considerable interest for applications involving high-quality-factor (high-Q) nanocavities because these structures can selectively confine light of various wavelengths. PhC L3 nanocavities with high-Q factors and a small cubic-wavelength volume are used for all-optical switching [8], low-threshold lasing [4–6], cavity quantum electrodynamics [7, 10], and to control ultrafast laser pulses [24]. Their higher-order modes are important to efficiently pump nanocavity lasers [4] and to selectively excite quantum dots embedded within the cavity [25]. Recently, work on L3 PhC cavities surrounded by low-RI material cladding has mainly concentrated on maximizing the Q factor of the fundamental

✉ Lazhar Kassa-Baghdouche
    kassabaghdouche_lazhar@yahoo.com

1 Département Electronique et Télécommunication, Faculté des Sciences et de la Technologie, Université 8 Mai 1945, 24000 Guelma, Algeria

2 Laboratoire Microsystèmes et Instrumentation (LMI), Faculté des Sciences et de la Technologie, Université Constantine 1, 25000 Constantine, Algeria

mode, with the specific aim of optimizing the ratio of Q factor to modal volume. To achieve mechanical stability of L3 cavities in 2D PhCs with low-RI cladding, some papers have reported the Q factors of structures with full and asymmetric cladding [15, 16, 22, 23]. By using organic polymer cladding, a resonant mode with a Q factor of 14,000 was designed in PhC L3 cavity with low-RI material cladding on a silicon wafer substrate [15]. A fully clad PhC L3 nanocavity completely embedded in glass (with all holes infiltrated by the glass) was numerically analyzed and a Q factor of 1100 was obtained [16]. In order to improve the Q factor of the cavities further, PhC cavities with symmetric solid and periodic low-RI cladding layers have recently emerged as a potential alternative to the cavities covered with low-RI material cladding [22]. For some applications may need SiO_2 or organic polymer clad PhC cavities, the Q factor of the designed cavities is higher than 10^4. While cavities with symmetric cladding have been studied, our previous work [23] presented an example of a L3 cavity with asymmetric low-RI material cladding. The designed hybrid L3 nanocavity is formed by infiltrating the air-hole array of the Si PhC with a polymer and depositing a polymer layer on top of the PhC membrane. This design resulted in a very high-Q factor due to the gentle confinement of the mode.

Asymmetric clad structures are inferior to fully clad structures in terms of vertical integration and protection against contamination because the asymmetric cladding breaks the symmetry of the structure around the device midplane, thereby adversely affecting its ability to classify modes as either even or odd and destroying the bandgap in the guided modes of the membrane [26]. Moreover, the vertical asymmetry degrades the performance of such photonic devices by decreasing the coupling between the transverse electric (TE) and transverse magnetic (TM) modes [14]. Finally, although PhC L3 cavities have been fully and partially clad with low-RI materials, ultrahigh-Q (i.e., comparable with air-bridge PhC nanocavities) nanocavities have yet to be realized in material-clad 2D PhCs.

In this paper, to improve heterogeneous integration and optimize the nonlinear properties, we analyze numerically a L3 cavity with various low-RI material claddings. The structures consist of a semiconductor membrane surrounded by low-RI material cladding for vertical confinement and 2D PhC for in-plane confinement. Because of the complex geometry of the structure and the large difference in RI, the calculations involve both full three-dimensional (3D) plane-wave expansion and 3D finite-difference time-domain (3D-FDTD) calculations. We compute the band diagram of 2D planar PhCs composed of a triangular lattice of air holes and investigate how the Q factors and resonant wavelengths depend on the RI of the cladding. Finally, by fine-tuning the radius and position of the air holes near the cavity edges, we analyze the optical properties of the proposed structures and modify their geometrical structure accordingly.

2 Cavity model and numerical method

Figure 1a shows the structure of interest, which is composed of a triangular lattice of air holes in a silicon membrane surrounded by air cladding. This structure was selected because of the high RI contrast of the air-bridge structure; the triangular lattice is used because a large bandgap appears for both the TE and TM polarizations for an infinitely thick membrane. A membrane with finite thickness supports guided resonances, which are strongly confined in the membrane and yet couple to free-space radiation through coherent Bragg scattering [26].

The optical characteristics of the proposed structure are studied by determining the characteristic photonic band structure. Toward this goal, the dispersion diagram, which shows the normalized frequency versus wave vector for TE- and TM-like modes, is given in Fig. 1b. The membrane thickness of the geometric structure is $h/a = 0.6$, and the hole radius is $r/a = 0.3$ (where a is the lattice constant of the PhC structure). The RI of the silicon membrane at 1.55 μm is $n_{Si} = 3.48$. The dispersion diagram was calculated for the Γ-K-M-Γ edge of the Brillouin zone. With a freely available software package [27], we computed the fully vectorial eigenmodes of Maxwell's equations with periodic boundary conditions by using preconditioned conjugate-gradient minimization of the block Rayleigh quotient in a plane-wave basis. For the chosen RI and a relatively small hole radius r, the band diagrams show a single-frequency bandgap for TE-polarized modes (even modes) but no gap for TM modes (odd modes). Also, in the dispersion diagram of Fig. 1b the fundamental bandgap is centered near a normalized frequency of 0.30 (a/λ). It extends between the normalized frequencies $\omega_1 = 0.254$ (a/λ) and $\omega_2 = 0.333$ (a/λ) for the waves with TE polarization.

The proposed donor-type point-defect cavity is made of triangular 2D PhC L-type cavities surrounded by two low-RI (n_{clad}) material claddings, which are formed by omitting three holes (L3) in a single row, as shown in Fig. 1c. This structure provides index guiding by total internal reflection in a direction normal to the plane of the crystal, as in a planar waveguide. We focus on 2D cavities with low-RI material cladding, which are more suitable for heterogeneous integration than those with air cladding. Suspended structures are considered symmetric, whereas 2D PhCs with a single-sided dielectric cladding are considered asymmetric. This type of structure was first realized as an air-bridge-type 2D PhC [28]: It offers very high-Q factors (Q factors of 45,000 and 88,000 were already demonstrated

Fig. 1 a Photonic crystal membrane structure patterned with a triangular lattice of air holes with its parameters defined. **b** Dispersion diagram for TE-like (*even modes*) and TM-like (*odd modes*) modes in a 2D planar photonic crystal composed of a triangular lattice of air holes with $r/a = 0.30$, $h/a = 0.6$, where a is the lattice constant of the 2D PhC. The PhC membrane has a bandgap in the TE-like mode. **c** Schematic illustration of a semiconductor 2D PhC L3 cavity surrounded by cladding layers made of low-RI material
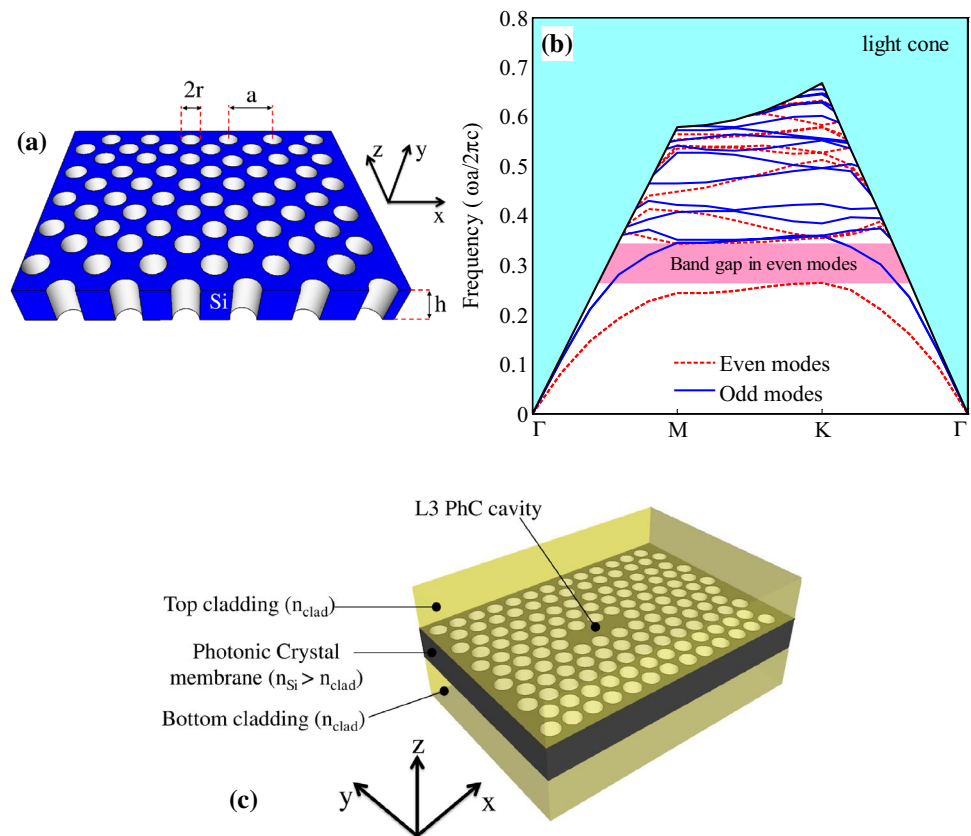
experimentally [28, 29], and lately, Lai et al. [30] measured that Q is approximately 2×10^6 and by varying the positions of few holes next to the defect, Minkov et al. [31] demonstrated that it is possible to systematically optimize L3 cavities to values of Q well above 10^6), and it is of great interest for applications requiring strong interactions between cavity and source, for quantum information processing, and for making low-threshold nanosource lasers, ultrasmall filters, or photonic chips.

To investigate the optical properties (i.e., Q factor and resonant wavelength) of cavities, we simulated electromagnetic waves by using a 3D-FDTD algorithm [32] implemented in a freely available software package with subpixel smoothing for increased accuracy [33]. To extract the resonance frequency and the cavity Q factor of the simulated structures, we used a filter diagonalization method [34]. In our 3D-FDTD calculation, the structure was illuminated at normal incidence by a Gaussian pulse with a TE-polarized mode. The simulated zone was surrounded by a perfectly matched layer of unit thickness, which absorbed the fields leaving the simulated region to prevent reflections. To accurately estimate the Q factor, the convergence of the solution was analyzed as a function of the size of the spatial domain. The Q factor, thus obtained, was used to determine the energy loss per cycle versus the energy stored and also the reflection loss at the interface between the interior and

exterior of the cavity for a material cavity with no absorption. All calculations were restricted to TE-like modes with significant electric-field components along the x and z directions (see Fig. 1a).

3 Results and discussion

3.1 Dependence of 2D PhC L3 cavity on refractive index of cladding

A number of key parameters have a significant impact on the optical properties of cavities made in planar PhCs, such as the holes radius, membrane thickness, and RI of both the membrane and cladding materials. Furthermore, 2D PhC structures should be supported by a low-RI material (as opposed to air). In practice, better mechanical stability and thermal management are obtained by covering the structure with a low-RI material cladding [35]. In addition, the dependence of the bandgap on the membrane thickness was investigated for three membrane structures with different claddings [36], with the results suggesting that, when deeply drilled oxide is used as the bottom cladding of a PhC, the bandgap frequencies are almost the same as for a PhC suspended in air. Thus, an air-bridge-type PhC can be converted to a low-RI cladding PhC without losing

Fig. 2 *Side view* of various designs proposed for a planar photonic crystal L3 cavity with various low-RI cladding for analysis and simulation. **a** Design A uses solid-symmetric cladding. **b** Design B uses fully symmetric cladding. **c** Design C uses periodic-symmetric cladding. **d** Design D uses asymmetric cladding
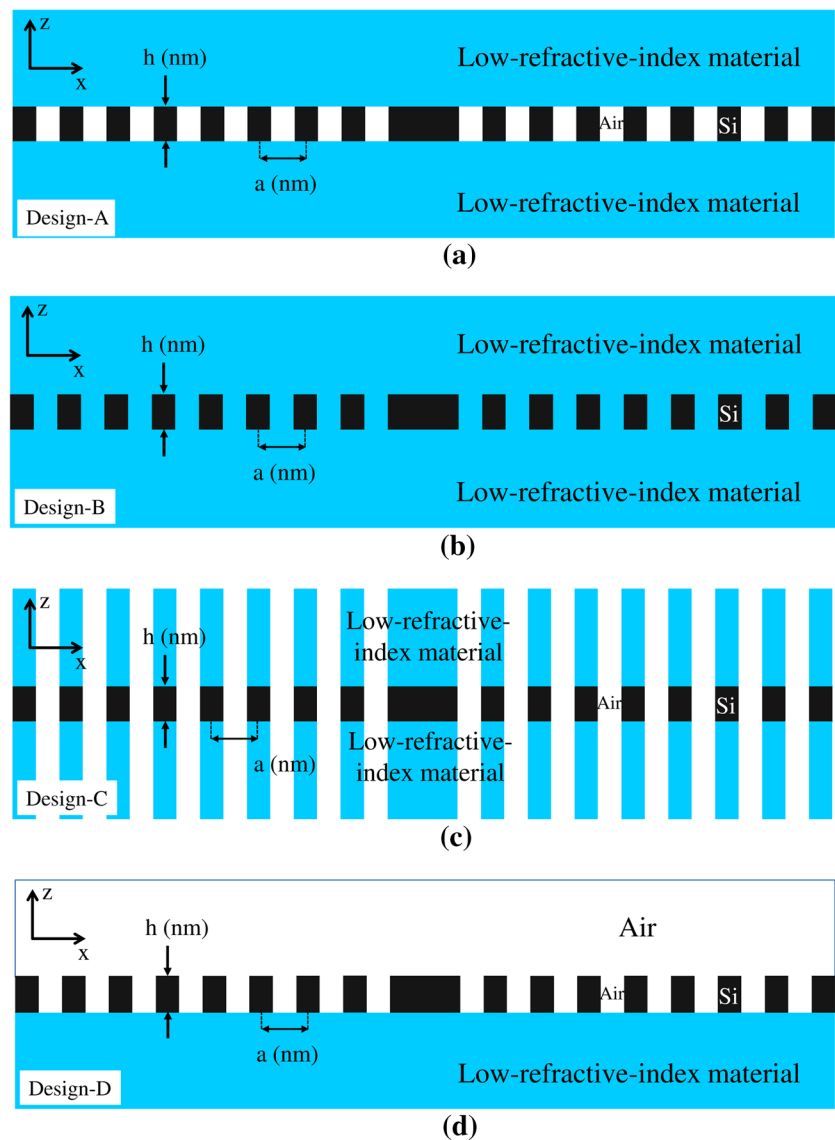
its frequency properties. However, if the membrane is on a uniform cladding, the bandgap frequencies may decrease significantly. Yet, for high-Q cavity modes, the presence of a low-RI cladding inevitably increases the vertical loss toward the cladding because the low-RI cladding layer produces an enlarged light cone in k space for the 2D PhC, thereby enhancing the coupling from resonant modes to radiation modes. Consequently, with low-RI cladding, the Q value is still expected to decrease. To minimize this effect, we consider in this section 2D PhC L3 cavities with different low-RI claddings. These structures are expected to have more desirable thermal and mechanical properties.

Figure 2 shows a schematic side view of four designs for PhC-based structures (designs A–D) that we analyzed and simulated. These designs are being implemented experimentally. In design A (Fig. 2a), the cladding materials above and below the membrane consist of a uniform low-RI material,

thus forming a symmetric cladding or "sandwich" (i.e., a symmetrically solid-clad cavity). The holes in design A are air filled. In design B (Fig. 2b), the silicon membrane is completely buried in a low-RI material cladding, so the low-RI material extends through the cladding and array of holes (i.e., a symmetrically fully clad cavity). Design C consists of a heterostructure; the effective index above and below the membrane is less than that of designs A and B because of the "extruded," low-RI membrane, as shown in Fig. 2c. In this structure, the holes extend through the low-RI cladding and through the membrane (i.e., a symmetric periodic-clad cavity). In addition, the index contrast between the core and cladding is high, and the mode profiles are quite extended. To maintain mirror symmetry, we focus on having the same low-RI material above and below the membrane. Finally, design D is a hybrid often found in silicon-on-insulator–based systems. The lower cladding usually consists of an
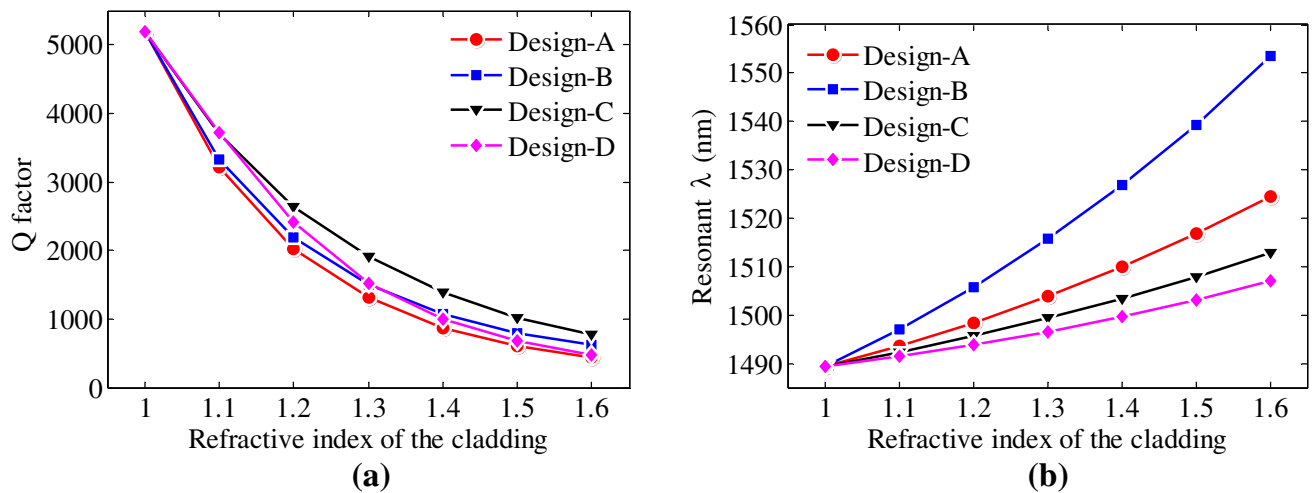
Fig. 3 **a** Q factor and **b** resonant wavelength of the various simulated 2D PhC L3 cavity modes (i.e., designs A–D) as a function of RI of the cladding

oxide layer, not necessarily structured, and the upper cladding usually consists of air (i.e., an asymmetrically clad cavity). The asymmetry of the mode profile within the structure may lead to additional losses. Due to limitations associated with fabrication, this structure usually has only a very thin upper cladding, yielding an asymmetrical mode profile. To avoid strong additional losses, this mode-profile asymmetry is often partly compensated for by choosing a lower cladding material with a dielectric constant smaller than that of the upper cladding.

These structures (i.e., designs A–D) can be integrated onto a chip more easily than can an air-bridge structure. For an oxide layer, the effective RI in the cladding is close to unity, so the associated structure may be easily integrated. As elaborated in the preceding section, the PhC is composed of silicon, and claddings are composed of low-RI material. Studying these designs should lead to a better understanding of the significant variation of Q factors with respect to the Q factor of the air-cladding structure. These structures are analyzed and compared in the next section. Moreover, from the viewpoint of fabrication, these designs can be easily fabricated [14, 16, 18, 20, 21]. An asymmetric PhC structure with L3 point-defect cavities was fabricated using SOI substrates [14]. The PhC structure was first formed in the Si membrane by electron-beam lithography and induction-coupled plasma reactive ion etching techniques. Then, in the case of the air-bridge structure, the lower SiO_2 layer was removed by HF wet etching, whereas the lower SiO_2 layer was left in the case of the SOI structure. A glass-embedded silicon photonic crystal device consisting of a broad bandwidth waveguide and a nanocavity with a high-quality (Q) factor was fabricated on a SOI wafer using spin-on glass (SOG) [16]. The photonic

crystal patterns were formed in the silicon layer using electron-beam lithography and plasma etching. Subsequently, a SOG of hydrogen silsesquioxane with tunable and low refractive indices was coated on the fabricated structure and cured at a temperature of 400 °C for 1 h under nitrogen atmosphere. Consequently, the SOG uniformly coats the surface and infiltrates the holes up to a depth of 530 nm from the silicon surface. Further, a symmetrically glass-clad Si 2D PhC nanocavity was fabricated using Si on the insulator wafer and SOG of hydrogen silsesquioxane [18].

To estimate the functionality of the proposed designs, the RI of the cladding materials, n_{clad}, is assumed to be low. In the simulation, this is done by changing the RI of the cladding from 1 (i.e., air) to 1.6 (i.e., organic polymer). Figure 3 plots the Q factor and resonant wavelength as a function of cladding RI. This plot clearly indicates that a maximum Q factor occurs at RI = 1.0 for all designs (air-bridge-type structure). Moreover, with the claddings, Q still decreases dramatically from that of an air-bridge-type structure (i.e., the cladding RI increases from 1 to 1.6, and the low-RI cladding goes close to the membrane), optical confinement by total internal reflection weakens, and Q decreases greatly. For example, Q is about 7.5 times lower for a low-RI value of $n = 1.54$ (corresponding to a polymer material). Recalling that Q for the L3 mode is highly sensitive to the cladding RI (considering the loss introduced by claddings), we see that design C has the highest Q of the four designs. Specifically, Q for the fundamental resonant mode of design C increases by a factor of approximately 1.5 relative to that for designs A, B, and D. Design A has the lowest Q because the cladding above and below the membrane consists of a uniform low-RI material. Q for design D is of the same order of magnitude as that for design A. Because Q is more sensitive to the

cladding RI, the cladding RI must remain less than the effective index of the membrane to retain an ultrahigh Q, so index guiding still produces high Q. Therefore, high Q can be achieved using a symmetrically periodic cladding. Figure 3b shows the variation of the resonant wavelength for the various designs as a function cladding RI. For the in-plane direction, 2D PhCs confine light via the PBG effect, so the slopes of the resonant wavelength curves are not equal; this suggests that the resonant wavelengths of the different designs do not have the same sensitivity to the RI of the cladding.

3.2 Adjustment of hole positions and radius in PhC L3 cavities with different low-RI material cladding

L3 cavities with low-RI material cladding offer the advantages of passivation, vertical stacking, mechanical strength, and heterogeneous integration. Although optical
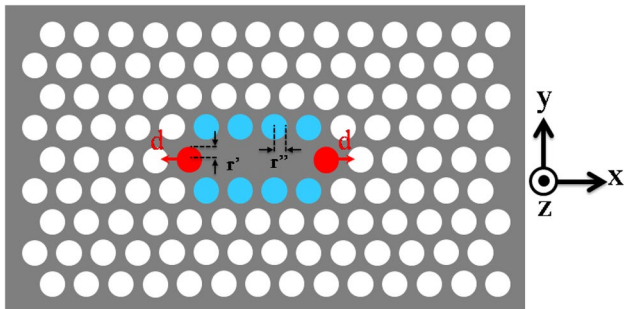

Fig. 4 L3 cavity structure designed by displacing the holes through a distance d and reducing their radius to r' at both edges of the defect to obtain a high Q factor. Additionally, the radius r'' of the *upper* and *lower holes* is reduced

confinement in the vertical direction is weak and the Q factor of the fundamental resonant mode decreases dramatically, the latter can be increased by using a momentum-space design, which allows the radiative component of the confined photonic mode to be reduced and minimizes propagation losses [28, 29]. In real space, this corresponds to changing the position or size of the nearby holes. Therefore, in this section, we discuss geometrical optimizations of the proposed designs with SiO_2 cladding ($n_{clad} = 1.44$) in which we fine-tune the positions and radius of air holes at both edges of the cavity.

First, the radius r′ of the left- and right-boundary air hole is reduced, and then they are shifted outward by a distance d (see Fig. 4). It was found that, upon decreasing the radius of the single hole, the Q factor does not improve significantly. However, upon increasing the hole displacement, the Q factor increases. Thus, the dependence of the resonant-mode properties (i.e., the Q factor and resonant wavelength) on the displacement d for hole radii $r' = 80$ nm are shown in Fig. 5 for designs A–D. The calculated variations in Q factor as the air holes are displaced are qualitatively similar for all designs. In other words, the Q factor increases considerably with hole displacement, reaches a maximum, and then decreases, in agreement with theoretical and experimental results [28, 29]. This figure show that a high-Q factor is obtained by using design C, which results in Q as large as 8500. When the hole radius $r' = 80$ mm and the hole displacement $d = 90$ nm, the calculated Q factor of design C is greater than that for designs A, B, and D (the Q factor is increased by a factor of 2.5 to approximately a value of 8832). The increase in the Q factor for the symmetrically periodic-clad cavity with displaced holes is explained as follows: If the holes were displaced
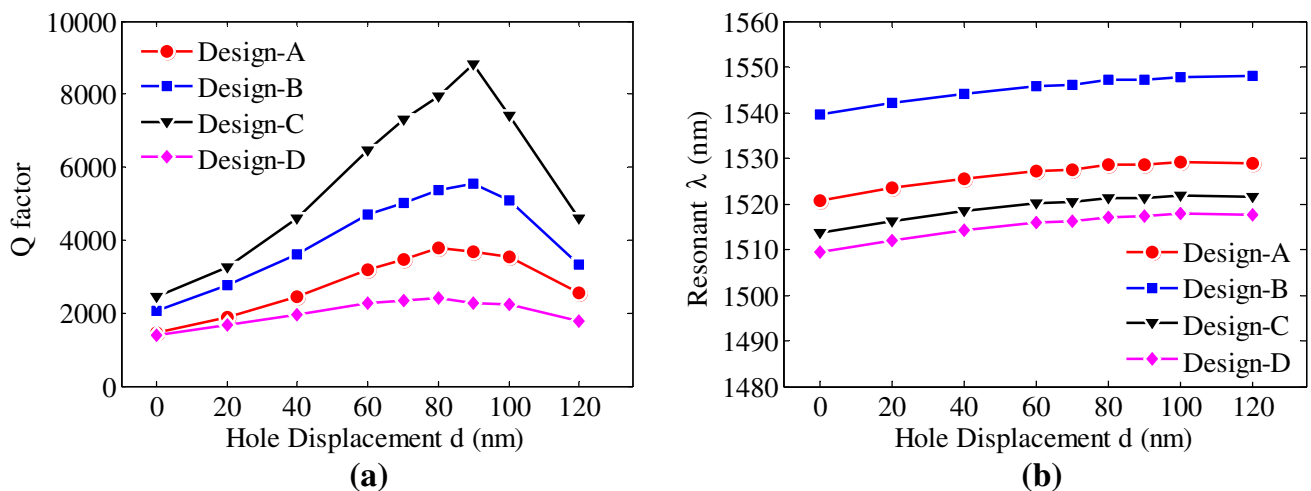

Fig. 5 **a** Q factor and **b** resonant wavelength for L3 cavity mode (designs A–D) versus displacement d of single air holes for reduced air-hole radii $r' = 80$ nm
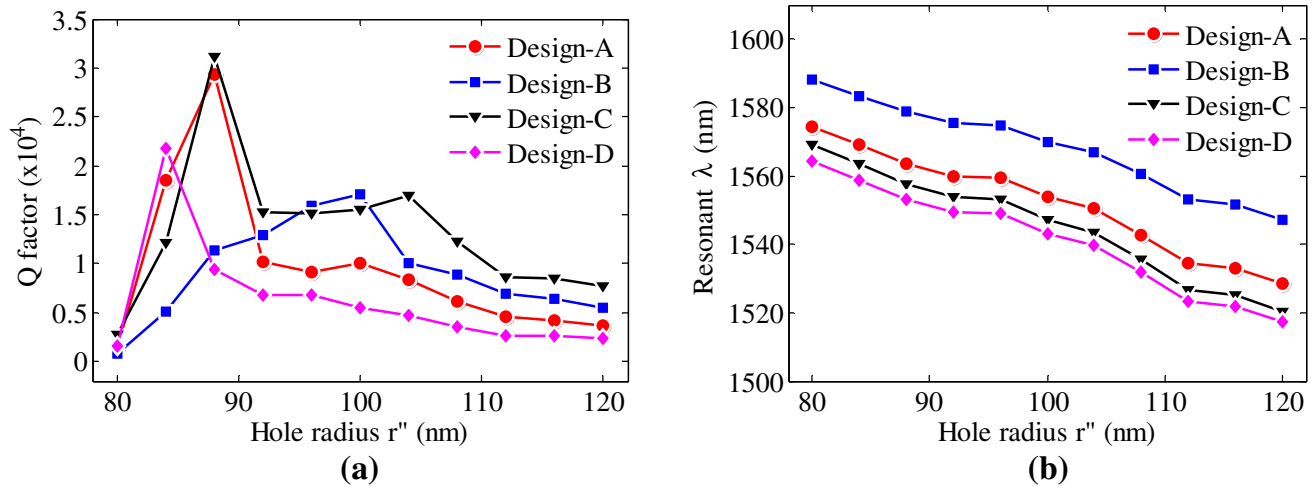
Fig. 6 Q factor and resonant wavelength for L3 cavity mode (designs A–D) versus radius r'' of upper- and lower-boundary air holes

to a great extent, then the electric field would reach farther outside the displaced holes. In this case, the optical confinement would be more gradual around the holes, whereas the electric field distribution would decay abruptly outside the holes. However, the envelope of the cavity electric field approaches a Gaussian function.

Second, the geometry of the cavity is modified by reducing the radius r'' of the upper- and lower-boundary holes of the defect while fixing the displacement d of the edge air holes and their radius r' at the optimum values for each design. The resulting Q factor and resonant wavelength for designs A–D are shown in Fig. 6, and the corresponding Q factors are displayed in a bar graph in Fig. 7. Figure 6a clearly indicates that, upon reducing the hole radius r'', the cavity Q factor increases significantly to a maximum and then decreases for a small cavity volume. This result clearly indicates that the Q factor for the designed cavities increases by a factor as large as 25 ($Q > 10^4$) relative to the Q factor for a cavity with air holes in their original position and with their original size. The Q factor increases by a factor of 39 ($Q = 29\,300$) for design A and 25 for designs B–C ($Q = 17{,}087$, $31{,}100$, and $21{,}700$, respectively). Figure 7 shows that design C results in the highest Q factor of the various designs: For $r'' = 88$ nm, a maximum of $Q = 3 \times 10^4$ occurs at the resonant wavelength $\lambda = 1557$ nm. This large Q factor is most likely due to the fluctuations in the geometrical structures, including symmetric cladding and extended holes, which lead to less scattering and coupling losses to TE-like membrane modes. Although displacing holes is thought to disturb the electromagnetic field and cause radiation loss, the disturbance and radiation loss are sufficiently small for design C. Moreover, the wavelength of the fundamental resonant mode in the various optimized designs also decreases upon finely
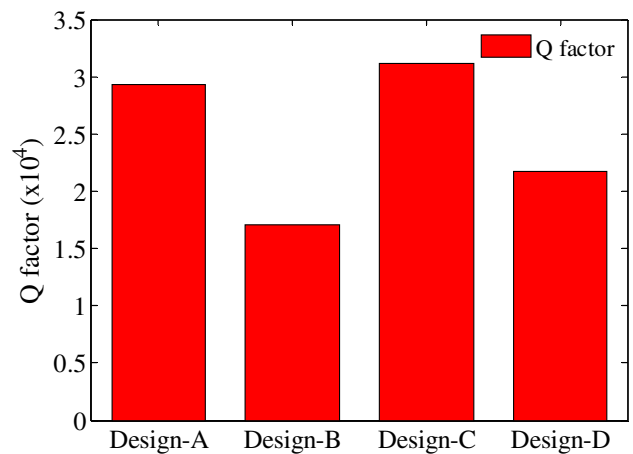

Fig. 7 Q factor for the various optimized designs

reducing the hole radius r'' (see Fig. 6b). The resonant wavelength for design A is slightly greater than the those for designs B and C, which indicates clearly that the cavity Q factor is further increased by tailoring the position and radius of air holes closest to the defect while keeping the cavity volume small. Thus, adjusting the position and radius of air holes is an effective technique for optimizing the Q factor of 2D PhC cavities with air-cladding and with low-RI materials. As shown by Fig. 7, design C has a reasonably high-Q factor and thus is suitable for integration with other photonic integrated circuits.

The proposed designs generally have an index contrast between membrane and cladding that is obtained by using cladding material different from the core material. The ideal structure would be a system with periodic-symmetric low-RI claddings (design B), which simultaneously leads to strong light confinement, simple integration, and

perfectly symmetrical mode profiles. From an experimental point of view, the periodic low-RI claddings should lead to low scattering losses. In the cladding, the air-filling fraction is greater, which lowers the effective RI. Therefore, design C (Fig. 2c) is the most promising design for future applications because it allows the PhC to be integrated onto a chip and simultaneously offers a high-Q factor and limited radiation losses. Furthermore, this design could be implemented at low cost by standard silicon technology. The advantages arise both from ease of fabrication (i.e., both membrane and cladding can be etched at the same time) and from the confinement of resonant cavity modes, because localized modes do not couple that strongly with lower-RI cladding [26]. The periodicity of the cladding, however, does not produce useful PhC membrane effects by itself. Even if a bandgap appears in the cladding modes, it would lie at frequencies above the bandgap of the guided modes and would therefore not provide additional confinement. Thus, to obtain high-Q cavities when using low-RI cladding, design considerations may need to include optimizing Q factors; simply migrating from air-bridge-type designs may give undesirable results. Finally, because design C offers a superior Q factor and thermal and mechanical properties (with respect to the previously studied design), it may also be a promising structure for implementing planar PhC devices.

4 Conclusion

To enhance the mechanical stability and the nonlinear properties of PhC cavities and maintain their excellent performance, we investigated how different low refractive index claddings affect planar high-Q PhC L3 cavities. We have shown theoretically that the Q factor of the fundamental resonant mode in the designed L3 cavity decreases significantly when the RI of the material cladding approaches that of the membrane (i.e., when the RI of the cladding is increased from 1 to 1.6). In addition, we have shown by numerical simulation that a periodic-symmetric distribution of the cladding material (i.e., design C) is critical for obtaining high-Q factors in a 2D planar PhC structure.

The higher Q factor enhances the coupling between resonant membrane modes and guided or radiation modes of the cladding, which lie outside the light cone of the planar PhC. We further improve the Q factor of PhC L3 cavities with low-RI material cladding by fine-tuning the position and radius of the lateral-, upper-, and lower-boundary holes near the cavity edges; this approach allows us to increase Q by a factor as large as 25. Although the resonant mode is considered to be derived from the leaky line-defect mode above the light line, a resonant mode with a high-Q factor ($Q > 10^4$) and small modal volume can be achieved. These

design rules can be used to fine-tune the optical properties of PhC cavities with low-RI material, which would be beneficial for applications requiring heterogeneous integration and nonlinear enhancement.

References

1. S.H. Fan, P.R. Villeneuve, J.D. Joannopoulos, E.F. Schubert, High extraction efficiency of spontaneous emission from slabs of photonic crystals. Phys. Rev. Lett. **78**, 3294–3297 (1997)
2. D. Englund, D. Fattal, E. Waks, G. Solomon, B. Zhang, T. Nakaoka, Y. Arakawa, Y. Yamamoto, J. Vučković, Controlling the spontaneous emission rate of single quantum dots in a two-dimensional photonic crystal. Phys. Rev. Lett. **95**, 013904-1–013904-4 (2005)
3. O. Painter, R.K. Lee, A. Scherer, A. Yariv, J.D. O'Brien, P.D. Dapkus, I. Kim, Two-dimensional photonic band-gap defect mode laser. Science **284**, 1819–1821 (1999)
4. M. Nomura, S. Iwamoto, K. Watanabe, N. Kumagai, Y. Nakata, S. Ishida, Y. Arakawa, Room temperature continuous-wave lasing in photonic crystal nanocavity. Opt. Express **14**, 6308–6315 (2006)
5. J. Hendrickson, B.C. Richards, J. Sweet, S. Mosor, C. Christenson, D. Lam, G. Khitrova, H.M. Gibbs, T. Yoshie, A. Scherer, O.B. Shchekin, D.G. Deppe, Quantum dot photonic-crystal-slab nanocavities: quality factors and lasing. Phys. Rev. B **72**, 193303 (2005)
6. M. Nomura, S. Iwamoto, M. Nishioka, S. Ishida, Y. Arakawa, Highly efficient optical pumping of photonic crystal nanocavity lasers using cavity resonant excitation. Appl. Phys. Lett. **89**(16), 161111 (2006)
7. H. Takano, B.-S. Song, T. Asano, S. Noda, Highly efficient multi-channel drop filter in a two-dimensional hetero photonic crystal. Opt. Express **14**, 3491–3496 (2006)
8. K. Nozaki, T. Tanabe, A. Shinya, S. Matsuo, T. Sato, H. Taniyama, M. Notomi, Sub-femtojoule all-optical switching using a photonic-crystal nanocavity. Nat. Photonics **4**(7), 477–483 (2010)
9. T. Yoshie, A. Scherer, J. Hendrickson, G. Khitrova, H.M. Gibbs, G. Rupper, C. Ell, O.B. Shchekin, D.G. Deppe, Vacuum Rabi splitting with a single quantum dot in a photonic crystal nanocavity. Nature **432**(7014), 200–203 (2004)
10. K. Hennessy, A. Badolato, M. Winger, D. Gerace, M. Atature, S. Gulde, S. Falt, E.L. Hu, A. Imamoglu, Quantum nature of a strongly coupled single quantum dot-cavity system. Nature **445**, 896–899 (2007)
11. S. Strauf, K. Hennessy, M.T. Rakher, Y.-S. Choi, A. Badolato, L.C. Andreani, E.L. Hu, P.M. Petroff, D. Bouwmeester, Self-tuned quantum dot gain in photonic crystal lasers. Phys. Rev. Lett. **96**, 127–404 (2006)
12. W.-H. Chang, W.-Y. Chen, H.-S. Chang, T.-P. Hsieh, J.-I. Chyi, T.-M. Hsu, Efficient single-photon sources based on low-density quantum dots in photonic-crystal nanocavities. Phys. Rev. Lett. **96**(11), 117401 (2006)
13. M. Borselli, T.J. Johnson, O. Painter, Measuring the role of surface chemistry in silicon microphotonics. Appl. Phys. Lett. **88**(13), 131114 (2006)
14. Y. Tanaka, T. Asano, R. Hatsuta, S. Noda, Investigation of point-defect cavity formed in two-dimensional photonic crystal slab

with one-sided dielectric cladding. Appl. Phys. Lett. **88**, 011112 (2006)

15. M. Okano, T. Yamada, J. Sugisaka, N. Yamamoto, M. Itoh, T. Sugaya, K. Komori, M. Mori, Design of two-dimensional photonic crystal nanocavities with low-refractive-index material cladding. J. Opt. **12**, 015108 (2010)

16. S.-W. Jeon, J.-K. Han, B.-S. Song, S. Noda, Glass-embedded two-dimensional silicon photonic crystal devices with a broad bandwidth waveguide and a high quality nanocavity. Opt. Express **18**, 19361–19366 (2010)

17. E. Kuramochi, H. Taniyama, T. Tanabe, K. Kawasaki, Y.-G. Roh, M. Notomi, Ultrahigh-Q one-dimensional photonic crystal nanocavities with modulated mode-gap barriers on SiO$_2$ claddings and on air claddings. Opt. Express **18**, 15859–15869 (2010)

18. B.-S. Song, S.-W. Jeon, S. Noda, Symmetrically glass-clad photonic crystal nanocavities with ultrahigh quality factors. Opt. Lett. **36**, 91–93 (2011)

19. Z. Han, X. Checoury, L.-D. Haret, P. Boucaud, High quality factor in a two-dimensional photonic crystal cavity on silicon-on-insulator. Opt. Lett. **36**, 1749–1751 (2011)

20. X. Gai, B. Luther-Davies, T.P. White, Photonic crystal nanocavities fabricated from chalcogenide glass fully embedded in an index-matched cladding with a high Q factor (>750,000). Opt. Express **20**, 15503–15515 (2012)

21. K. Welnaa, M. Huguesb, C. P. Reardona, L. O'Faolaina, M. Hopkinsonb, T. F. Kraussa, Photonic crystal nanocavities in GaAs/AlGaAs with oxidised bottom cladding. Photonics Nanostruct. Fundam. Appl. **11**(2), 139–144 (2013)

22. L. Kassa-Baghdouche, T. Boumaza, M. Bouchemat, Planar photonic crystal nanocavities with symmetric cladding layers for integrated optics. Opt. Eng. **53**(12), 127107 (2014)

23. L. Kassa-Baghdouche, T. Boumaza, M. Bouchemat, Optimization of Q-factor in nonlinear planar photonic crystal nanocavity incorporating hybrid silicon/polymer material. Phys. Scr. **90**, 065504 (2015)

24. T. Asano, W. Kunishi, B.-S. Song, S. Noda, Time-domain response of point-defect cavities in two dimensional photonic crystal slabs using picosecond light pulse. Appl. Phys. Lett. **88**, 151102 (2006)

25. M. Nomura, S. Iwamoto, T. Yang, S. Ishida, Y. Arakawa, Enhancement of light emission from single quantum dot in photonic crystal nanocavity by using cavity resonant excitation. Appl. Phys. Lett. **89**(24), 241124 (2006)

26. S.G. Johnson, S. Fan, P.R. Villeneuve, J.D. Joannopoulos, L. Kolodziejski, Guided modes in photonic crystal slabs. Phys. Rev. B **60**(8), 5751–5758 (1999)

27. S. Johnson, J.D. Joannopoulos, Block-iterative frequency-domain methods for Maxwell's equations in a planewave basis. Opt. Express **8**, 173–190 (2001)

28. Y. Akahane, T. Asano, B.S. Song, S. Noda, High-Q photonic nanocavity in a two-dimensional photonic crystal. Nature **425**, 944–947 (2003)

29. Y. Akahane, T. Asano, B.S. Song, S. Noda, Fine-tuned high Q photonic crystal nanocavity. Opt. Express **13**, 1202–1214 (2005)

30. Y. Lai, S. Pirotta, G. Urbinati, D. Gerace, M. Minkov, V. Savona, A. Badolato, M. Galli, Genetically designed L3 photonic crystal nanocavities with measured quality factor exceeding one million. Appl. Phys. Lett. **104**, 241101 (2014)

31. Momchil Minkov, V. Savona, Automated optimization of photonic crystal slab cavities. Sci. Rep. **4**, 5124 (2014)

32. A. Taflove, S.C. Hagness, *Computational Electrodynamics: The Finite-Difference Time-Domain Method*, 3rd edn. (Artech House, Norwood, 2005)

33. A.F. Oskooi, D. Roundy, M. Ibanescu, P. Bermel, J.D. Joannopoulos, S.G. Johnson, MEEP: a flexible free-software package for electromagnetic simulations by the FDTD method. Comput. Phys. Commun. **181**, 687–702 (2010)

34. V.A. Mandelshtam, H.S. Taylor, Harmonic inversion of time signals. J. Chem. Phys. **107**, 6756–6769 (1997)

35. H.-Y. Ryu, H.-G. Park, Y.-H. Lee, Two-dimensional photonic crystal semiconductor lasers: computational design, fabrication, and characterization. IEEE J. Sel. Top. Quantum Electron. **8**(4), 891–908 (2002)

36. H.-Y. Ryu, J.-K. Hwang, Y.-H. Lee, Conditions of single guided mode in two dimensional triangular photonic crystal slab waveguides. J. Appl. Phys. **88**(9), 4941–4946 (2000)